RSC Advances

Facile synthesis of highly ordered mesoporous cobalt-alumina catalysts and their application in liquid phase selective oxidation of styrene

Journal:	*RSC Advances*
Manuscript ID	RA-ART-10-2015-020531.R1
Article Type:	Paper
Date Submitted by the Author:	30-Oct-2015
Complete List of Authors:	Pan, Dahai; Taiyuan University of Technology, The Research Center of Chemical Technology & Catalysis for Energy Li, Ruifeng; Taiyuan University of Technology, Xu, Qian; Taiyuan University of Technology, Dong, Zhaoyang; Taiyuan University of Technology, Chen, Shuwei; Taiyuan University of Technology, Yu, Feng; Taiyuan University of Technology, The Research Center of Chemical Technology & Catalysis for Energy Yan, Xiaoliang; Taiyuan University of Technology, College of Chemistry and Chemical Engineering Fan, Binbin; Taiyuan University of technology,
Subject area & keyword:	Inorganic materials < Materials

RSC Advances

PAPER

Facile synthesis of highly ordered mesoporous cobalt-alumina catalysts and their application in liquid phase selective oxidation of styrene

Received 00th January 20xx,
Accepted 00th January 20xx

DOI: 10.1039/x0xx00000x

www.rsc.org/

Dahai Pan,* Qian Xu, Zhaoyang Dong, Shuwei Chen, Feng Yu, Xiaoliang Yan, Binbin Fan and Ruifeng Li *

A series of highly ordered mesoporous cobalt-alumina catalysts (denoted as OMCA-x) with a variety of n_{Al}/n_{Co} ratios have been successfully synthesized via the evaporation-induced triconstituent cooperative co-assembly method and were applied to the liquid phase selective oxidation of styrene using difficult-to-activate molecular oxygen as oxidant at atmospheric pressure. For comparison, a cobalt catalyst with the n_{Al}/n_{Co} ratio of 10 supported on ordered mesoporous alumina (denoted as Co/OMA-10) was also prepared by a traditional incipient wetness impregnation (IWI) method. Although both kinds of catalysts retained unidimensionally ordered mesoporous structure, textural and catalytic properties of the catalysts were significantly affected by the preparation methods. The characteristic and catalytic results confirmed that OMCA-x catalysts exhibited much more highly ordered hexagonal mesostructure, narrower pore-size distribution, higher Brunauer-Emmett-Teller surface area and pore volume, and higher catalytic activity and selectivity to styrene oxide than those of Co/OMA-10. The improved catalytic activity of OMCA-x catalysts can be attributed to the highly homogeneous dispersion of Co species within mesoporous alumina framework in the form of tetrahedrally coordinated divalent Co-oxide moieties, which can efficiently activate molecular oxygen into peroxo and superoxo radical-type active oxygens. In addition, the incorporation of Co into the mesoporous framework of alumina and the formation of Co-O-Al bond can effectively increase the content of tetra- and penta-coordinated framework aluminum, and further facilitate the formation of tetrahedrally coordinated Ia type Al-OH species as the catalytic centers for styrene epoxidation, which are advantageous to improve the selectivity for styrene oxide.

1. Introduction

Catalytic oxidation of styrene at the side chain has a significant industrial impact because it produces a series of useful functionalized chemicals, including styrene oxide and benzaldehyde, which are important and versatile synthetic intermediates in chemical industry.[1] Especially, styrene oxide is a commercially important intermediate used for the synthesis of different fine chemicals and pharmaceuticals.[2, 3] However, being a terminal olefin, styrene is difficult to oxidize, since the desired product (styrene oxide) is intermediate in a sequence of reactions, which is easily oxidized into benzaldehyde or phenylacetaldehyde, and over oxidation further results in a series of undesired by-products.[4] Conventionally, styrene oxide is synthesized either by dehydrochlorination of styrene chlorohydrin with a base or oxidation of styrene using organic peracids.[5-7] All these methods used hazardous chemicals and showed poor selectivity for styrene epoxide, thus not only leading to the generation of undesirable products but also resulting in a huge amount of toxically corrosive chemical wastes. In the past years, to replace the conventional route for oxidation of styrene, great efforts have been made to develop environmentally friendly reusable heterogeneous catalysts such as TS-1,[8, 9] Co/CNs,[10] Ti/SiO_2,[11] Au_n superatoms,[12] γ-Al_2O_3,[13] CeO_2,[3] Ga_2O_3,[14] encapsulated V, Cu and Ni complexes,[15-17] and La, V, Cr, Mn, Cu, Ni, and Ti modified molecular sieves,[18-20] using tert-butyl hydroperoxide (TBHP),[10, 12, 19] H_2O_2,[8, 15, 18, 21] or urea-H_2O_2 adduct [9] as oxidant. Although styrene conversion is very high when H_2O_2 is used as an oxidant, the selectivity for styrene oxide is poor.[22] On the other hand, using TBHP [11] and urea-H_2O_2 adduct [23] as oxidants yields high styrene oxide selectivity (>80%) with low styrene conversion (9.8 and 17.7%, respectively).

Molecular oxygen is the most desirable oxidant for the epoxidation of alkenes due to the inherent advantages being cheap, readily available, and ensuring a high atom economy, thus, there has recently been an increased interest in the oxidation of styrene using molecular oxygen to produce styrene oxide or benzaldehyde.[2, 21, 24] Despite these advantages, molecular oxygen is difficult to be activated due to its higher dissociation energy than those of H_2O_2 and other organic hydroperoxides, and it remains a challenge to use molecular oxygen effectively for partial oxidations of olefin

The Research Center of Chemical Technology & Catalysis for Energy, College of Chemistry and Chemical Engineering, Taiyuan University of Technology, Taiyuan 030024, China. E-mail: pandahai@foxmail.com (D. H. Pan), rfli@tyut.edu.cn (R. F. Li); Fax: +86-351-6010121

while limiting the production of by-products. It is well known that transition metals, especially cobalt containing catalysts, can efficiently catalyze the oxidation of organic substrates (e.g. styrene) with O_2,[2, 25, 26] which produces valuable organic intermediates in perfumeries, dyestuffs and pharmaceuticals. Various supported Co catalysts, including Co^{2+}-exchanged zeolites,[2, 27] Co-substituted mesoporous materials,[28, 29] cobalt supported on silica,[26, 30] and Co immobilized in metal organic framework[31] have been developed to enhance the epoxidation of alkene. Previous results revealed that the catalytic performances of Co-based catalysts are closed to the nature, ordination, location and dispersion of cobalt species, which depend strongly on the support, Co loading, and method of preparation.[32-34] The high dispersion of metal ions as isolated species on the support with an ordered structure and pore dimensions resulted in the excellent properties of cobalt catalysts.[28, 35] Therefore, a better understanding of the structural properties (e.g. cobalt state, nature of cobalt species, and porous structure) with regard to catalytic applications in oxidation of styrene is strongly required to enable the design of efficient mesoporous catalysts.

Ordered mesoporous alumina (OMA) as a nonpolluting material with highly uniform channel, large surface area, narrow pore-size distribution, and tunable pore size should possess much more excellent properties for the use as desired carrier in the selective oxidation of styrene. Unfortunately, typical recipes for the preparation of ordered mesoporous silica do not work effectively for the synthesis of alumina analogues, due to the fast hydrolysis and condensation rates of aluminum precursor and phase transitions accompanied by the thermal breakdown of the structural integrity during calcination process to remove organic templates,[36-38] which often result in the formation of disordered alumina with poor thermal stability. At present, OMA materials are commonly synthesized by the following general pathways: (1) by solvent-deficient synthesis without the structure-directing agents or templates,[39, 40] (2) by adopting the nanocasting method with silica or carbon molds as hard templates,[41-43] and (3) a pathway based on a modified sol–gel self-assembly process in the presence of a soft template such as cationic, anionic, or nonionic surfactant as the structure-directing agent (SDA).[44-47] Compared with the first two pathways, the modified sol-gel self-assembly method is a very attractive alternative way to synthesize alumina materials with well-defined mesostructural, textural, morphological, and chemical properties which are extremely desirable for application in heterogeneous catalysis. In 2005, Niesz et al.[47] reported the successful synthesis of OMA using block copolymers as the soft template for the first time, i.e. the origin of pathway (3). Since then, a significant breakthrough has been realized following this general pathway by using the $EO_{20}PO_{70}EO_{20}$ triblock copolymer (P123) as the soft template in ethanol solution with hydrochloric acid or nitric acid as pH adjustor.[44] This route is called the solvent evaporation induced self-assembly (EISA). In such method, self-assembled micelle structure is induced by increasing the micelle concentration through evaporation of solvent. Unidimensionally OMA or alumina-supported metal oxides are formed by removing cylindrical micelle assembly through thermal decomposition of micelle.[48] Obviously, EISA method can effectively obviates the necessity to strictly control hydrolysis conditions of aluminum precursors to synthesize OMA materials in an easy and reproducible manner, and competently substitute the process of cooperative assembly of precursors and surfactant templates typically employed to afford mesoporous materials. According to previous studies, [49-51] the OMA support with high surface area can remarkably increase the dispersion of active metal particles and effectively prevent their aggregation and sintering by the so-called confinement effect of mesopores during high temperature calcination and catalytic reaction. In other words, the activity and selectivity of catalysts can be improved by finely dispersing active metal throughout the mesoporous alumina supports. Therefore, developing an ordered meoporous cobalt-alumina catalyst for the selective oxidation of styrene with molecular oxygen as oxidant would be of great interest.

Recently, we have reported that introducing heteroatoms into the framework of mesoporous alumina may bring many different kinds of new materials and excellent novel properties.[38, 52] Inspired from our previous works, herein we propose a feasible approach to the synthesis of highly ordered mesoporous cobalt-alumina (OMCA-x) catalysts with a variety of n_{Al}/n_{Co} ratios. For comparison, a cobalt catalyst supported on OMA support was also prepared by a traditional incipient wetness impregnation (IWI) method. The prepared catalysts were applied to the selective oxidation of styrene to styrene oxide with oxygen as the sole oxidant. The effects of preparation method of cobalt-alumina catalysts on their physicochemical properties and catalytic performances were investigated. By correlating the cobalt state and mesostructural properties of cobalt-alumina catalysts with activity and selectivity for styrene oxide, a synergetic effect of highly homogeneously dispersed Co^{2+} in tetrahedral position and remarkably increased Ia type Al-OH species as the catalytic centers was provided to understand the improved styrene conversion and selectivity for styrene oxide over OMCA-x catalysts.

2. Experimental

Chemicals

Triblock copolymer F127 (M_w=12600, $EO_{106}PO_{70}EO_{106}$) was purchased from Sigma-Aldrich. Aluminum isopropoxide, cobalt nitrate hexahydrate, citric acid (CA), hydrochloric acid (HCl), and anhydrous ethanol were obtained from Tianjin Chemical Reagent Co.. In addition, styrene, 1,4-dioxane, methylbenzene, and chlorobenzene were obtained from Beijing Reagent Co.. All of the chemicals were of analytical grade and used as received without further purification.

Synthesis for ordered mesoporous cobalt-alumina catalysts

The OMCA-x catalysts were synthesized by a single-step EISA method associated with thermal treatment, according to a

similar method described in the literatures.[38, 52] Fig. 1 shows the schematic procedure for the preparation of OMCA-x catalysts. In a typical synthesis, 3.2 g of F127 was dissolved in 20 mL anhydrous ethanol solution containing 0.4 g of citric acid and 1.6 g of 37 wt% hydrochloric acid. Then, 3.26 g of aluminum isopropoxide and a required amount of cobalt nitrate hexahydrate (0.15, 0.23, 0.46 and 0.93 g, respectively) were slowly added into the above solution, simultaneously. After being vigorously stirred at 32 °C for 24 h, the resultant mixture was transferred to a dish and underwent solvent evaporation at 45 °C for 48 h and thermal treatment at 100 °C for 24 h, respectively. The final products were calcined at 400 °C for 5 h at a heating rate of 1 °C/min to remove the template and named as OMCA-x, where x stands for the molar ratio of Al/Co.

For comparison, the OMA support was prepared without adding the cobalt precursor, according to the similar method described above. A cobalt catalyst supported on OMA was prepared by an IWI method. 1.0 g of OMA was added into 40 mL anhydrous ethanol solution dissolved 0.284 g of cobalt nitrate hexahydrate. The resultant mixture was stirred at 32 °C for 24 h and then dried at 100 °C for 12 h. The final sample was calcined at 400 °C for 5 h at a heating rate of 1 °C/min. According to the molar ratio of Al/Co, the prepared catalyst was named as Co/OMA-10.

Catalyst characterization

Power X-ray diffraction (XRD) analysis of catalysts was performed on a Shimadzu XRD-6000 diffractometer using Ni-filtered Cu Kα (0.154 nm) radiation. Transmission electron microscopy (TEM) experiments were performed on a JEOL JEM-2100F microscope operated at 200 kV. Samples were dispersed in ethanol by moderate sonication. Then, a carbon-coated Cu TEM grid was dipped in the sample suspension and dried under vacuum at 80 °C before analysis. The elemental mapping was performed on a Hitachi Model S-4800 high-resolution fluoresence-emission scanning electron microscopy instrument, using an acceleration voltage of 25 kV. Nitrogen adsorption-desorption isotherms were measured on a Quantachrome analyzer at -196 °C. Before measurements, the samples were degassed at 180 °C in vacuum for 10 h. The Brunauer-Emmett-Teller (BET) method was used to calculate the specific surface areas. The pore volumes and pore size distributions were derived from the adsorption branches of the isotherms using the Barrett-Joyner-Halenda (BJH) method. The total pore volume, V_P, was calculated from the amount of nitrogen adsorbed at a relative pressure of 0.99. The UV-vis spectra of prepared catalysts were collected on a Varian Cary 300 UV-Vis spectrophotometer coupled with a diffuse reflectance accessory. The surface composition of catalysts were determined from X-ray photoelectron spectroscopy (XPS) performed by an ESCALAB 250 spectrometer with a monochromatized Al K source (1486.6 eV) at the constant analyzer pass energy of 30.0 eV. The binding energy is estimated to be accurate within 0.1 eV. All binding energies (BEs) were corrected referencing to the C 1s (284.6 eV) peak of the contamination carbon as an internal standard. The Co 2p binding energy of the core level was determined by computer fitting of the measured spectra. Hydrogen temperature-programmed reduced (H_2-TPR) measurements for catalysts OMCA-x and Co/OMA-10 were performed in a quart fixed-bed microreactor. Before the H_2-TPR measurements, 0.1 g of samples were pretreated at 300 °C for 1 h in flowing high purity helium (30 mL/min) to remove any moisture and other impurities adsorbed in the samples. After cooling to 200 °C, the sample was exposed to a flow (30 mL/min) of 10% H_2-Ar and heated at a rate of 10 °C/min to 800 °C, and the hydrogen consumption was measured using a thermal conductivity detector (TCD). ^{27}Al MAS NMR spectra were recorded on a Bruker AVANCE^{III} 6000Hz instrument operated at frequency 156.37 MHz, pulse width 3.98 μs, pulse delay 4 s, acquisition time 0.014 s, and spinning rate 8 kHz for 3072 scans. The content of cobalt in catalyst was determined by atomic absorption spectroscopic analysis on a Thermo Elemental SOLAAR S2 spectrometer.

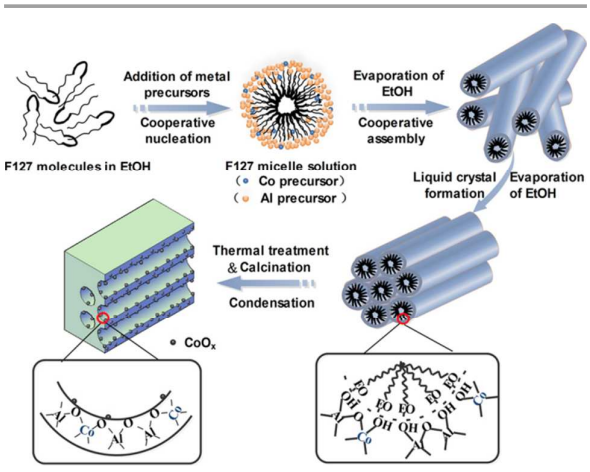

Fig. 1 The schematic procedure for the preparation of catalysts OMCA-x.

Catalytic reactions

The catalytic reaction for styrene oxidation was carried out in a 50 mL two-necked round-bottom glass flask connected to a reflux condenser and a thermometer. The temperature of the reaction vessel was maintained using an oil bath. In a typical reaction, styrene (1.0 g) and solvent 1,4-dioxane (15 mL) were added to the flask, containing 0.04 g of catalyst under stirring (600 rpm). The reaction was initiated by bubbling O_2 at atmospheric pressure into the reaction mixture at the rate of 8-10 mL/min. Chlorobenzene was used as the internal standard. After 5 h of reaction at 90 °C, the mixture was cooled down to room temperature and the catalyst was separated from the reaction mixture by centrifugation. The oxidation products were analyzed on a gas chromatograph (DANI) equipped with a flame ionization detector (FID) and a RTX-1 capillary column. After each styrene oxidation run, the catalyst was cooled to room temperature, separated by

centrifugation from the product solution, washed with 1,4-dioxane several times, dried at 200 °C for 24 h for complete removal of organics and unreacted styrene molecules, and reused for the next run under the same reaction conditions. Herein, the conversion of styrene was calculated by internal standard method, and the turnover frequency (TOF) was calculated as follow:

$$\mathrm{TOF} = \frac{\text{No. of moles of styrene oxide formed}}{\text{No. of moles of cobalt in the catalyst} \times \text{reaction time}}$$

3. Results and discussion

Crystalline structures of support (OMA) and catalysts (OMCA-x and Co/OMA-10) were investigated by XRD measurements. It is well-known that the diffraction patterns at small angles provide information about the possible organization of mesopores.[53] As can be seen in Fig. 2a, the XRD features of catalysts OMCA-x (except for OMCA-5) are rather similar to support OMA, with two well-resolved Bragg peaks. Using the catalyst OMCA-10 as an example, a very strong diffraction around 0.86 ° and one weak peak around 1.56 ° were observed, which, according to the TEM observation (Fig. 3a and b), can be indexed as the (100), (110), and (200) reflections associated with a highly ordered two-dimensional (2D) hexagonal mesostructure (space group *p6mm*). Compared with the XRD pattern of support OMA, catalysts OMCA-30 and OMCA-20 showed relatively stronger intensity of (110) and (200) peaks and narrower full width at half-maximum (FWHW) as judged from the (100) diffraction peak in their XRD patterns, suggesting that the divalent Co species from the hydrolysis of cobalt nitrate hexahydrate can participate in and promote the cooperative self-assembly between F127 and aluminum species to construct a uniform mesoporous framework in which oligomers of cobalt and aluminum species cross-link together to form the Co-O-Al bond during the thermal and calcination treatment (Fig. 1), leading to a remarkably increased mesostructural ordering. However, for catalysts OMCA-10 and OMCA-5 prepared with a further increase in Co loading, the intensity of (110) and (200) diffractions relative to that of (100) diffraction decreased gradually, corresponding to a less regularity of mesopores. Especially, catalyst OMCA-5 only showed one diffraction peak and failed to show periodic arrangement of the mesoporous organization. Due to the detection limitation of the XRD technique, no signals of cobalt oxides were detected in the wide-angle XRD pattern of OMCA-5 (Fig. 2b). In other words, it is hard to be conclusive if all added Co species had been homogeneously incorporated into the mesoporous framework of alumina or existed in the mesoporous channels of alumina in the form of cobalt oxides nanoparticles. Nonetheless, high resolution TEM technique is much more effective than XRD technique in detecting the distribution of Co species, and the results so obtained are helpful to identify the position of Co species in OMCA-5 as illustrated later in Fig. 3c. From Fig. 2a, it also can be seen that with increasing the introduced amount of Co, there is a distinct shift in the position of the (100) diffraction peak, which could be used to support the assumption that Co species have participated in the cooperative self-assembly between F127 and aluminum species and been incorporated into the framework of alumina during the synthesis. It is interesting to note that with the increase in the molar ratio of Al/Co from 5 to ∞ (OMA, prepared without adding Co precursor), the first diffraction peak of OMCA-x was shifted toward lower angle

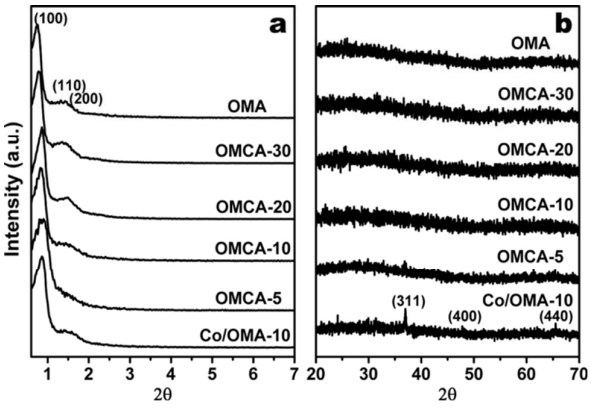

Fig. 2 Small- (a) and wide- (b) angle XRD patterns of OMA support and cobalt-alumina catalysts prepared with different methods.

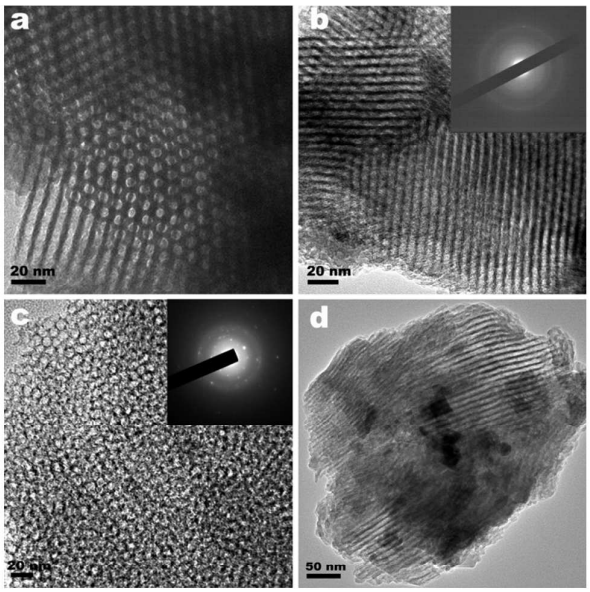

Fig. 3 TEM images (a) and (b) of OMCA-10 viewed along [100] and [110] orientations, TEM images of OMCA-5 (c) and Co/OMA-10 (d) viewed along [100] and [110] orientations, respectively (the insets in b and c are the corresponding SAED patterns of OMCA-10 and OMCA-5, respectively).

Table 1. The physicochemical properties of OMA support and cobalt-alumina catalysts prepared with different methods.

Catalyst	n_{Al}/n_{Co}	a_0 (nm)	S_{BET} (m^2/g)	V_P (cm^3/g)	D_P (nm)
OMA	∞	13.8	229	0.51	11.5
OMCA-30	30	12.7	294	0.74	11.5
OMCA-20	20	12.2	305	0.74	11.6
OMCA-10	10	12.1	289	0.59	8.6
OMCA-5	5	11.6	247	0.45	7.6
Co/OMA-10	10	12.7	198	0.50	9.8

a_0, Unit cell parameter; S_{BET}, specific surface area; V_P, total pore volume; D_P, pore diameter.

(Fig. 2a), representing an increase in the lattice parameter (d_{100}) values. Through the calculation using the equation $a_0 = 2d_{100}/3^{1/2}$, the unite cell parameters of 13.8, 12.7, 12.2, 12.1, and 11.6 nm can be obtained for OMA, OMCA-30, OMCA-20, OMCA-10, and OMCA-5, respectively (Table 1). The decrease of the *d*-values and a_0 of OMCA-x with increasing the Co loading can be attributed to the incorporation of Co^{2+} with smaller atomic radius than that of Al^{3+} into the mesoporous framework of alumina and the formation of Co-O bond with shorter length than that of Al-O bond during the preparation of catalysts OMCA-x. The similar phenomenon was also observed when different metal elements were incorporated into ordered mesoporous materials with 2D hexagonal mesostructure.[28, 54]

On the other hand, different from OMA support and OMCA-x catalysts, Co/OMA-10 synthesized using IWI method exhibited apparent decrease in the relative intensity of (110) and (200) peaks in its small-angle region, suggesting that there was a deterioration of the ordered mesoporous structure. In addition, weak diffraction peaks at ca. 37, 47, and 65 °, ascribed to the crystalline Co_3O_4, could be discerned in the wide-angle XRD pattern of Co/OMA-10 (Fig. 2b), indicating that the cobalt species introduced by the impregnation method were poorly dispersed and aggregated into Co_3O_4 particles. This is consistent with the TEM observation (Fig. 3d), which showed that although Co/OMA-10 could sustain the hexagonal mesoporous structure of support OMA to a certain extent, several Co_3O_4 particles with different sizes located on the external surface rather than within the mesoporous channels of OMA. The characteristic results from XRD and TEM indicate that it is difficult to finely disperse cobalt species on the surface or in the mesoporous walls of support OMA through the traditional IWI method.

It is well known that high resolution TEM images could provide a direct observation of mesostructural organization and the distribution of metal species on support. Here, we take OMCA-10 as an example, and use TEM analysis to illustrate catalysts OMCA-x (except for OMCA-5) with the highly ordered mesostructure. As shown in Fig. 3a and 3b, hexagonally packed cylindrical pores along [100] orientation and parallel channels along [110] orientation signify the typical 2D hexagonal mesostructure with uniform pore size and wall thickness. Judged from the white-dark contrast of TEM images, the distance between two neighboring mesochannels is ca. 10.5 nm, in good agreement with the value calculated from the XRD analysis (Fig. 2a and Table 1). The selective area electron diffraction (SAED) pattern (the inset in Fig. 2b) of the ordered mesostructured domains of OMCA-10 indicates the mesoporous wall is still amorphous phase, and further confirms that there is no crystal phase structure of cobalt oxides. In addition, under the mode of TEM, a cobalt signal can be clearly observed in the energy dispersive X-ray analysis (EDX) spectrum of OMCA-10 (not shown), which confirmed that a large amount of Co is present in the sample. When three different probe spots were selected, the Al/Co molar ratios calculated from the EDX data were 11.3, 12.1, and 11.6, respectively, all of which are similar to that of original molar ratio of 10. This indicates that almost all Co species added in the initial reaction mixture have been eventually introduced into the final catalyst (OMCA-10) with a result of the highly homogeneous distribution of Co and Al at atomic level. The expected highly homogenous distribution of elements within the framework of OMCA-10 was further confirmed by the density of the O, Al, and Co sports in the elemental mapping (Fig. 4). For example, three different regions of OMCA-10 were scanned, and O, Al, and incorporated Co were found. The atomic ratios of Al to Co, analyzed in these three regions, are 12.7, 12.1, and 10.7, respectively. In comparison with the theoretical molar ratio of Al/Co in the precursor solution, this ratio in the final catalyst varies slightly, depending on the selected region. However, with further increasing the Co amount, the TEM image of OMCA-5 (Fig. 3c) confirmed the disordered mesostructure. The selective area electron diffraction pattern (the insert in part c of Fig. 3) of OMCA-5 further revealed the existence of several crystalline

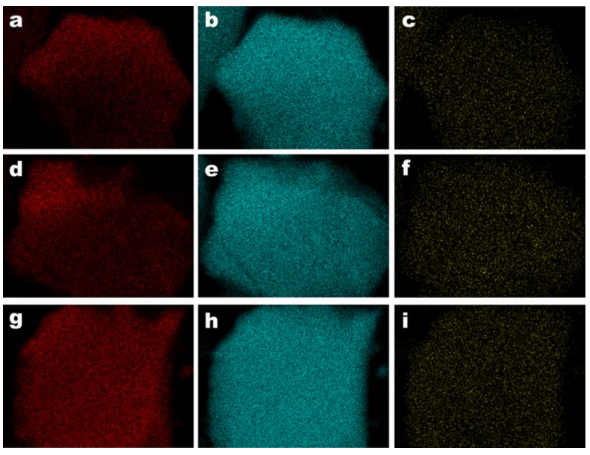

Fig. 4 Elemental analysis mapping for three different regions of catalyst OMCA-10 showing the distributions of O (a, d, g), Al (b, e, h), and Co (c, f, i). Maps in each row are for the same region.

nanoparticles. Considering absence of crystalline structure with alumina or cobalt oxide in the mesoporous wall of OMCA-10 (the inset in Fig. 3b), we attribute these nanoparticles to the crystalline Co_3O_4 homogenously existing in the mesoporous walls and channels, which could be confirmed by the later characteristic results from UV-vis, XPS, H_2-TPR, and ^{27}Al MAS NMR. Such observation could be probably originated from the excessive Co atomic diffusion and sintering during the calcination process at high temperature, and the forming process of Co_3O_4 nanoparticles may be the main reason for resulting in the partial collapse of ordered mesostructure of OMCA-5 (Fig. 2a).

The N_2 adsorption-desorption isotherms and corresponding pore size distribution curves of support (OMA) and catalysts (OMCA-x and Co/OMA-10) are shown in Fig. 5. The detailed textural properties derived from these isotherms are summarized in Table 1. Fig. 5a shows that all samples displayed IV-type isotherms with H1-type hysteresis loops, suggesting the presence of cylindrical mesopores. Compared with OMA, OMCA-x (except for OMCA-5) demonstrated a steeper capillary condensation step occurred at a relative pressure (P/P_0) ranging from 0.60 to 0.80, corresponding to a narrower pore size distribution (Fig. 5b), indicating that the incorporation of a required amount of Co ($n_{Al}/n_{Co} \geq 10$) can effectively increase the mesoporous uniform of alumina materials, which was consistent with the effect of the incorporation of Co on the mesostructural ordering of alumina (Fig. 2a). It is noticeable that the capillary condensation step is shifted to lower relative pressure with increasing Co content in catalysts OMCA-x (Fig. 5a), corresponding to a decrease of pore diameter from 11.6 to 7.6 nm (Table 1). The decrease in pore size with increasing Co loading amount once again manifests that more cobalt ions have been incorporated into the mesoporous framework of alumina because of the shorter bond length of Co-O than that of Al-O. Moreover, for catalysts OMCA-x prepared with the incorporation of Co, there are distinct increases in the other textural properties such as specific surface area and pore volume compared with those of OMA (Table 1). When the molar ratio of Al to Co is 20, both specific surface area and pore volume reach the largest, which are 305 m^2/g and 0.74 cm^3/g, respectively. Such result further verifies that the divalent Co species from the hydrolysis of cobalt precursor have participated in and promoted the cooperative self-assembly between F127 and aluminum species to form much more ordered mesostructure (Fig. 2a), taking into account the same introduction amount of Al precursor in each OMCA-x catalyst as that of OMA. However, the very high Co-containing mesoporous catalysts (OMCA-10 and OMCA-5) show the gradual decrease in specific surface area and pore volume, which are 289 and 247 m^2/g, 0.59 and 0.45 cm^3/g for OMCA-10 and OMCA-5, respectively. This trend is not only due to the transition to a less ordered mesoporous structure with incorporating the higher Co content (Fig. 2a), but also to the intrinsic effect of the 2.18 times higher atomic mass of Co compared to that of Al. When taking into account this factor, the specific surface area and pore volume of OMCA-10 are comparable to those of OMCA-20.

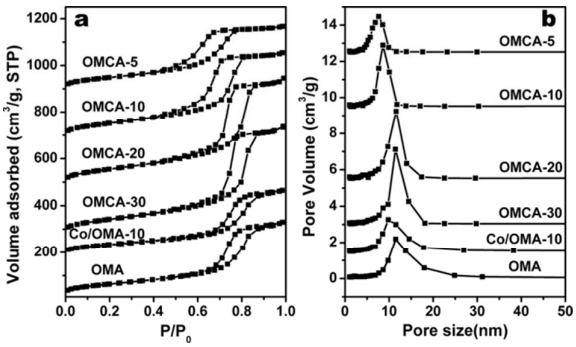

Fig. 5 N_2 sorption isotherms (a) and the corresponding pore size distribution curves (b) of OMA support and cobalt-alumina catalysts prepared with different methods. For clarity, in (a), the isotherms of Co/OMA-10, OMCA-30, OMCA-20, OMCA-10, and OMCA-5 are offset along the Y-axis by 220, 260, 470, 670, and 880 cm^3/g, respectively. In (b), the pore size distributions are correspondingly offset by 1.5, 3.0, 5.5, 9.5, and 12.5 cm^3/g, respectively.

Different from catalysts OMCA-x, for catalyst Co/OMA-10 prepared with the tradition IWI method, there are no obviously changes in the isotherm and the pore size distribution curve before and after impregnating cobalt (Fig. 5), which indicates that almost all of Co species exist on the external surface of support OMA rather than highly homogeneously disperse in the mesoporous channels of support OMA (Fig. 3d). As a result, Co/OMA-10 showed lesser specific surface area and pore volume as compared with OMA support (as shown in Table 1).

The diffuse reflectance UV–vis spectroscopy is known to be a very sensitive probe for identification of metal ion existence in the framework of metal-containing mesoporous materials. Fig. 6 depicts the diffuse reflectance UV-vis spectra of OMA, Co/OMA-10, and OMCA-x to investigate the local environment of cobalt ions in catalysts. There is no absorptive peak in the wavelength range of 200–800 nm for OMA sample, while OMCA-x exhibited three absorptive peaks located at ca. 510, 590 and 645 nm, which were caused by Jahn-Teller distortions and/ or spin-orbit coupling during the spin-allowed $^4A_2 \rightarrow {}^4T_1$ transition.[55] The position of these bands suggested the tetrahedrally coordinated Co^{2+} existing in the framework of mesoporous alumina.[29] Additionally, it can be observed that the relative intensity of these three absorptive peaks gradually increases with an increase in cobalt content in catalysts OMCA-30, OMCA-20, and OMCA-10, which provides another proof of incorporation of Co into mesoporous framework of alumina. However, for OMCA-5 prepared with further increasing the incorporation amount of Co, the relative intensity of triplet at 510, 590 and 645 nm decreased remarkably, and another broad band at 750 nm, attributed to absorbance of Co_3O_4 clusters,[56] was also detected. This indicates that a large amount of Co^{2+} species enriched on the surface of OMCA-5 were partially agglomerated into Co_3O_4 nanoparticles existing

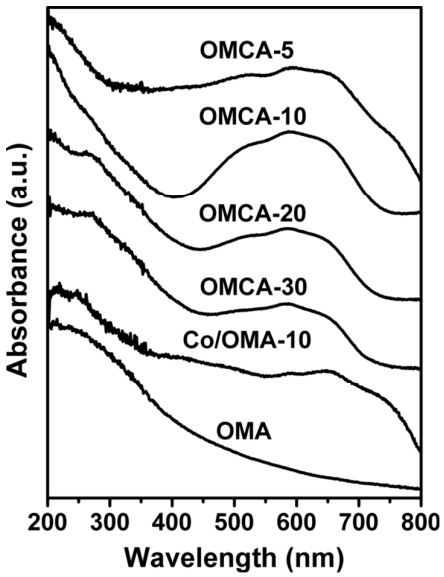

Fig. 6 UV-vis spectra for OMA support and cobalt-alumina catalysts prepared with different methods.

in the mesoporous walls or channels of alumina during the synthesis and subsequent calcination process (Fig. 3c).

Some of Co ions incorporated in the mesoporous framework of alumina are distributed on the near surface, which may create a small amount of surface oxide and oxidized Co ions in the framework after calcination. Here, the Co 2p photoelectrons were detected using the X-ray photoelectron spectroscopy (XPS) to determine the oxidation state of the cobalt on the near-surface region of catalysts. Fig. 7 shows the Co 2p XPS spectra for three typical Co-containing catalysts (OMCA-10, OMCA-5, and Co/OMA-10). Two components due to spin-orbital splitting Co $2p_{3/2}$ and Co $2p_{1/2}$, along with two shoulders at their high binding energy side which can only be ascribed to the shake-up process of Co^{2+} compound in the high spin state, were observed. For all three catalysts, the binding energies of Co $2p_{3/2}$ and Co $2p_{1/2}$ peaks were 780.9 and 796.7 eV, respectively, corresponding to 15.8 eV of spin-orbital spitting upon ionization between $2p_{3/2}$ and $2p_{1/2}$. The Co $2p_{3/2}$ peak at 780.9 eV, accompanied by a relatively intense 3d→4s shake-up satellite peak at 786.3 eV, could be used to confirm the presence of Co(II) in an isolated state.[29, 55] It is interesting to note that the OMCA-10 displayed a very strong shake-up satellite, suggesting that the surface cobalt species are largely present as Co(II) in the single-site state. Compared to the XPS spectrum of OMCA-10, OMCA-5 prepared with further increasing the Co loading exhibited relatively higher signal-to-noise ratio in its XPS spectrum, indicating that more surface cobalt were detected by XPS; while the ratio of peaks area between Co $2p_{3/2}$ and its satellite was slightly higher than that of OMCA-10, demonstrating the presence of surface Co^{3+} ion with the low spin state, which does not show the shake-up process.[57] In addition, Co/OMA-10 prepared by the impregnation method with the same loading amount of cobalt as that of OMCA-10 exhibited an unconspicuous shake-up process, suggesting the formation of large Co_3O_4 particles.[35] This coincides with the observations from TEM (Fig. 3d) and UV-vis (Fig. 6).

The interaction between cobalt species and support in the different cobalt-alumina catalysts was examined by the temperature-programmed reduction (TPR) technique to further confirm the cobalt species having been incorporated into the mesoporous framework of alumina in catalysts OMCA-x prepared by our method. Fig. 8 shows the H_2-TPR profiles of OMA, Co/OMA-10 and OMCA-x. As shown in Fig. 8, under equal experimental conditions, no reduction band was observed over the support OMA. In the temperature range from 300 to 800 ^{o}C, three very broad and weak reduction bands centered at 360, 500, and 700 ^{o}C, respectively, were observed for catalyst Co/OMA-10, revealing that Co species were present in different forms. The first two low temperature reduction bands were typically assigned to the stepwise reduction of supported Co_3O_4 to CoO and then CoO to Co, while the broad reduction band discerned at ca. 700 ^{o}C could be ascribed to the reduction of a small part of surface isolated Co(II) and some small CoO_x clusters having been strongly interacted with the support OMA.[55] For OMCA-x (except for OMCA-5), however, only one reduction peak (>650 ^{o}C) was found, indicating no cobalt oxides particles existing on the surface of OMCA-x. In addition, OMCA-x catalysts showed much higher resistance against reduction reflected in the higher reduction temperature relative to Co species, further indicating that the cobalt species are highly homogeneously incorporated into the mesoporous framework of alumina. Interestingly, it is observed from Fig. 8 that with increasing cobalt loading, the reduction peak of OMCA-x is shifted gradually to lower temperature, companied with the larger

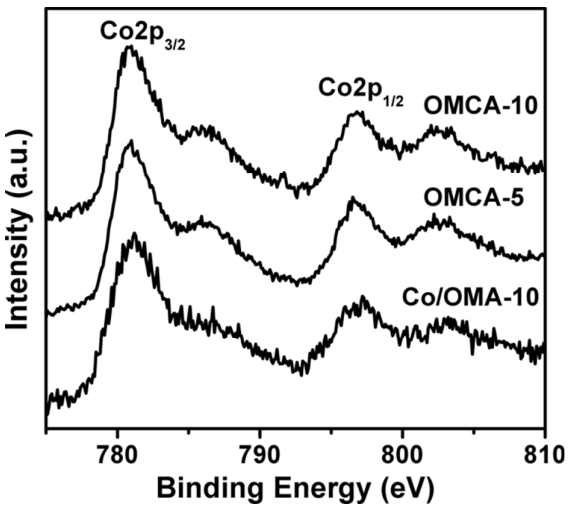

Fig. 7 XPS spectra of catalysts OMCA-10, OMCA-5 and Co/OMA-10.

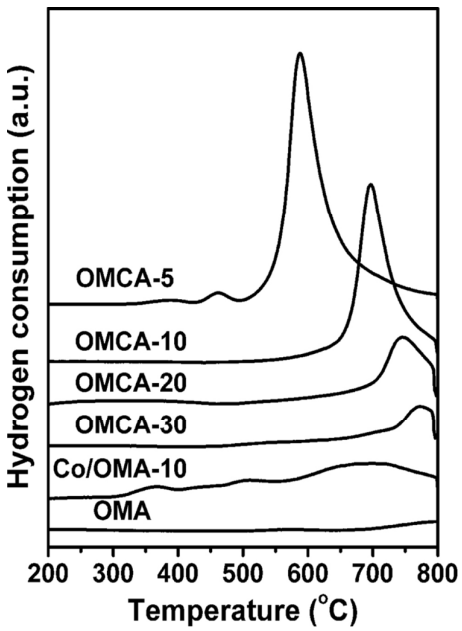

Fig. 8 H_2-TPR profiles of OMA support and cobalt-alumina catalysts prepared with different methods.

hydrogen consumption peak areas. The difference in reducibility of Co species incorporated into the mesoporous framework of alumina could be attributed to the different number of Al^{3+} ions in the Co surroundings. With the increase in the molar ratio of Al/Co during the synthesis of OMCA-x, the more Al^{3+} ions around Co atom will offer a much stronger polarization, which results in the poorer reducibility reflected in a higher reduction temperature.[56, 58] Different from other OMCA-x catalysts, the major reduction peak of OMCA-5 obviously shifted toward lower temperature, which was located at 588 °C; meanwhile, two small shoulders appeared at 380 and 460 °C, respectively. The possible explanation is that the formation of a large amount of cobalt oxides nanoparticles (including Co_3O_4) embedded in the mesoporous walls or on the inner surface of OMCA-5 (as seen in Fig. 3c), which weakens the strong interaction between cobalt species and alumina framework.

The above results from XRD, TEM, N_2 physisorption, UV-vis, XPS, and H_2-TPR suggest that a certain amount of Co species could be successfully incorporated into the mesoporous framework of alumina via our method, and the loading amount of Co can remarkably affect the structural and textural properties of resultant catalysts OMCA-x. In general, two main processes have been proposed to explain the formation of ordered mesoporous structure with surfactants as template. Firstly, the liquid crystal templating (LCT) mechanism,[59] in which the inorganic phase condenses around a stabilized surfactant mesophase. Secondly, the cooperative self-assembly (CSA) mechanism,[60] where the surfactant molecules and the inorganic species combine to form hybrid intermediate entities in a first step, which behave as independent surfactant species (the building blocks of the hybrid structure). Based on our results and former models, in our case, a triconstituent cooperative co-assembly process of inorganic divalent cobalt species from the hydrolysis of cobalt nitrate, aluminum oligomers hydrolyzed from aluminum isopropoxide, and amphiphilic triblock copolymer F127, was proposed to explain the formation of highly ordered mesoporous OMCA-x catalysts via the modified EISA route. The final nanocomposites possess a highly ordered mesostructure and uniform framework, in which oligomers of both cobalt and aluminum species cross-link together to form the bond of Al-O-Co. As a result, the cobalt species are highly homogeneously distributed in the mesoporous framework of alumina at the atomic level (Fig. 1).

First, the surfactant F127 molecules were dissolved in anhydrous ethanol solution containing a required amount of citric acid and hydrochloric acid, where the concentration of F127 was far less than its critical micelle concentration. The presence of citric acid, hydrochloric acid, and water from the 37 wt% hydrochloric acid can effective increase the polarity of the medium, which facilitate the folding of template. After the addition of cobalt and aluminum precursors, the hydroxyl group (-OH) of cobalt and aluminum from the controlled hydrolysis of cobalt nitrate and aluminum isopropoxide, respectively, can interact with the hydrophilic polyethylene oxide (PEO) of surfactant molecules through hydrogen bonding, which will promote the cooperative nucleation to form sphere-like micelles in which hydrophobic polypropylene oxide (PPO) remains in the core surrounded by hydrophilic PEO interacted with Co-OH and Al-OH in the corona. During the subsequent low temperature evaporation of solvent process, the progressively increasing the surfactant concentration drives the self-organization of micelles into cylindrical structures and further into periodic hexagonal mesophases in the presence of inorganic species, and finally leading to the form of ordered composite mesostructures. In the whole cooperative co-assembly process, the concentration of hydroxyl group (-OH) of cobalt and aluminum plays an important role in mesophase formation, and increasing the hydroxyl group (-OH) concentration of Co and Al can significantly enhance the hydrogen bonding interaction to further increase the mesostructural ordering of final materials. The use of anhydrous ethanol as solvent can strongly slow down the hydrolysis and condensation rate of inorganic precursors, which is highly beneficial for the formation of small inorganic oligomers with a large amount of hydroxyl group. In addition, hydrocarboxylic acids (such as citric acid) as an excellent coordination agents can behave as a ligand and bond with aluminum and cobalt atoms in a bidentate or bridging fashion. The complexation interaction between citric acid and alumina/cobalt species can effectively moderate the condensation reaction of inorganic oligomers in the solution. As a result, the addition of a required amount of citric acid can retain more Al-OH and Co-OH groups on the organic-inorganic interface, and thus enhance the cooperative self-assembly between F127 and aluminum/cobalt species by the hydrogen

bonding interaction. During further thermal treatment process at 100 ^{o}C, the composite mesostructure, i.e., ordered arrays of cylindrical micelles embedded within alumina and cobalt matrices, experiences further wall condensation and framework shrinkage with the support from the surfactant micelles within the mesoporous channels against the collapse of mesostructure. Meanwhile, Al-OH and Co-OH groups within mesoporous walls undergo the dehydroxylation and cross-link together to form Al-O-Co and Al-O-Al bonds. The followed calcination process at high temperature to remove the template micelles can further increase the cross-link degree of inorganic Al/Co species.

To underpin our proposed mechanism, the ^{27}Al MAS NMR spectra were used to provide direct evidence on the cross-linking of mesostructured cobalt-alumina materials synthesized by our method. Fig. 9 displays the ^{27}Al MAS NMR spectra of OMA, OMCA-x, and Co/OMA-10 calcined at 400 ^{o}C. The ^{27}Al MAS NMR spectrum of OMA presented three resonance signals at 4.6, 34.2, and 65.9 ppm, implying the presence of different oxygen environment surrounding aluminum sites. The peaks at 4.6 and 65.9 ppm are ascribed to the octa-coordinated (non-framework) aluminum (AlO_6) and the tetra-coordinated (framework) aluminum (AlO_4), respectively; while the peak at 34.2 ppm is attributed to the formation of penta-coordinated aluminum species (AlO_5), which results from the distortion of framework aluminum species that are particularly strained.[61, 62] In addition, the presence of a high concentration of pentahedrally coordinated aluminum also is a direct consequence of the high quantity of detects induced by the large surface area of the network.[63]

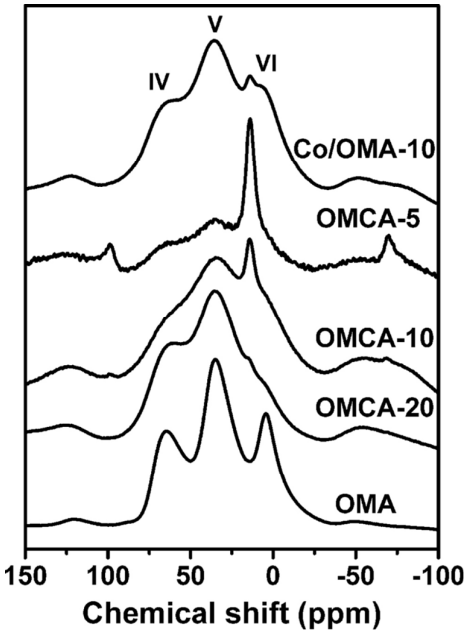

Fig. 9 ^{27}Al MAS NMR spectra of OMA support and cobalt-alumina catalysts prepared with different methods.

These three peaks are relatively wide due to quadrupole broadening. The proportions of tetra-, penta-, and octa-coordinated aluminum species were obtained by direct integration of the respective peaks after classical peak decomposition from the spectrum, which were 24.4, 48.8, and 26.6%, respectively. It is noteworthy that compared with OMA, OMCA-20 displayed a progressive increase in the intensities of the tetra- and penta-coordinated aluminums at the expense of the decrease in the intensity of octa-coordinated aluminum, corresponding to a higher relative population of AlO_4 and AlO_5 framework aluminum species from the cross-linkage between cobalt and aluminum hydroxyl species and the formation of Co-O-Al band within mesoporous walls during the thermal treatment and calcination process. After deconvolution, the ratio of $AlO_6/(AlO_4+AlO_5)$ calculated was 0.21, which was much lower than that (0.39) of OMA prepared without the incorporation of cobalt. However, gradually increasing cobalt content may affect the cooperative co-assembly between F127 and citric acid coordinated aluminum/cobalt species, leading to a gradual deduction in the intensities of tetra- and penta-coordinated aluminum species in the spectra observed for OMCA-10 and OMCA-5. The reason could be due to increasing incorporated cobalt content, the added adjacent hydroxyl groups of cobalt experienced dehydroxylation, diffusion and sintering to form small surface cobalt oxides within the mesoporous walls of alumina during the high temperature calcination process (Fig. 3c, 6, 7 and 8). As a result, a large amount of cobalt species were eliminated from the mesoporous framework, leading to the part collapse of ordered mesostructure of OMCA-10 and OMCA-5 and a remarkable increase in the octahedrally coordinated non-framework aluminum. The interaction between the produced surface cobalt oxides and unstable non-framework aluminum species would remarkably influenced the chemical environment of the octahedral-coordinated aluminum species, leading to the decrease in the intensity of peak at 4.6 ppm and the appearance of a new signal at 13.8 ppm, which could be attributed to the dynamic nuclear polarization (DNP) effect from the paramagnetic surface cobalt oxides to enhance the NMR signal of octahedral-coordinated aluminum by transferring the magnetization of unpaired electrons of cobalt to the nuclei of aluminum.[64] Different from support OMA and catalysts OMCA-x, the ^{27}Al MAS NMR spectrum of Co/OMA-10 prepared by the traditional IWI method displayed a relatively stronger resonance signal at 4.6 ppm and a very weak peak at 13.8 ppm, suggesting the original mesoporous structure of support OMA was destroyed partly to form more octahedrally coordinated aluminum species during the impregnating Co process. Meanwhile, the appearance of weaker peak at 13.8 ppm could probably be due to the poor dispersion of Co species and the formation of the larger cobalt oxides particles existing on the external surface of support OMA (Fig. 3d), which inevitably caused the obvious decrease in the surface area of cobalt oxides, and further decreased the interaction between surface cobalt oxides and non-framework aluminum species (Fig. 8).

The selective oxidation of styrene to styrene oxide has been carried out to investigate the catalytic properties of catalysts OMCA-x, and the catalyst Co/OMA-10 and support OMA for comparison. Table 2 summarizes the results of styrene oxidation over different catalysts with O_2 and 1,4-dioxane as oxidant and solvent, respectively. It is of interest to note that $Co(NO_3)_2$ is almost inactive for the conversion of styrene with O_2. We thus speculate that the epoxidation of styrene proceeds heterogeneously. The recent studies discovered that when hydrogen peroxide was used the oxidant, the terminal-hydroxyls bonded to four-coordinated Al(III) ions (type Ia Al-OH) are the active sites for the epoxidation of various nucleophilic olefins, which is attributed to that Al(III) ions in a four-coordinated environment are more capable of polarizing the peroxide ligand because its ionic radius is 53 pm, much smaller than that of six-coordinated Al(III) ions (68 pm).[13] In addition, regarding electronic aspects, four-coordinated Al(III) sites also more efficiently polarize the O-O bond, because they are more electron-deficient than six-coordinated Al(III) sites.[65] The generation of superficial hydroperoxides (Al-OOH) from the reaction between the Ia type Al-OH and H_2O_2, are responsible for distal oxygen transfer to the nucleophilic olefin.[13] In our reaction for oxidation of styrene, however, the oxygen is used as oxidant. It is difficult to directly activate oxygen by four-coordinated Al(III) sites from OMA, leading to a less catalytic activity. After calculation through GC analysis, the conversion of styrene and the selectivity of styrene oxide over cobalt-free OMA support only were 25.8% and 18.4%, respectively. In contrast, the introduction of cobalt into OMA can remarkably increase the conversion of styrene (above 78%) and the selectivity for styrene oxide (around 50%), with exception of Co/OMA-10 with large Co oxides particle size and less Co dispersion (Fig. 3d), which showed the lowest 36.8% of styrene conversion and 17.8% of selectivity to styrene oxide, among all cobalt-alumina catalysts. Evidently, the aggregated Co_3O_4 particles (Fig. 2b and Fig. 3d) as the main cobalt species existing the external surface of OMA showed the relatively lower catalytic activity for the epoxidation of styrene with O_2 as oxidant than that of highly homogeneously dispersed divalent Co^{2+} species as the signle-site active centres in the catalysts OMCA-x. Indeed, the divalent Co^{2+} species incorporated in the mesoporous framework of alumina in tetrahedral position (Fig. 6 and 7) are more stable and avoided the oxidation to higher oxidation states (e.g. Co_3O_4, Co_2O_3) (Fig. 8), in accordance with those observed for Co^{2+} exchanged zeolites.[66] Interestingly, for catalysts OMCA-x, with the increase of cobalt content, the obvious increases in the styrene conversion and selectivity to styrene oxide were found in Table 2. Catalyst OMCA-10 with the same loading amount of Co as that of Co/OMA-10 was apparently active for the reaction with the highest selectivity to styrene oxide (56.6 %). However, further increasing the introduced content of cobalt, for catalyst OMCA-5, a slight drop in the epoxide selectivity was observed, albeit the conversion of styrene was little higher than that (75.8 %) of OMCA-10. In addition, an obvious decrease in TOF value with increasing amount of cobalt loaded over catalysts OMCA-x was found in Table 2. For catalyst OMCA-30 with the lowest loading amount of Co, a TOF value of 110.7 for catalytic epoxide production could be attained although the styrene conversion is lower than other catalysts OMCA-x, which further indicates that the highly homogeneously dispersed divalent Co^{2+} species on OMA as the active site to the styrene epoxidation show very high catalytic efficiency.

The correlation of the catalytic properties of OMCA-x with the cobalt state and the amount of AlO_4 framework aluminum, we believe that a synergetic effect of highly homogeneously dispersed Co^{2+} in tetrahedral position and amount of Ia type Al-OH sites results in the remarkably high conversion of styrene and epoxide productivity. The mechanism of catalytic epoxidation of styrene with O_2 as oxidant over OMCA-x is not completely understood in our present work; however, we propose a tentative mechanism (Fig. 10) based on those reported by Sebastian et al.[2] and Rinaldi et al.[13]. The four-coordinated Co^{2+} cations presenting at surface or near-surface of mesopores in catalysts OMCA-x can firstly bind and activate oxygen to form Co(III)-(O_2^-) species, which undergo reactions to generate peroxo and superoxo active oxygen species with a radical nature.[55] The generated radical-type active oxygens could be easily received by solvent 1,4-dioxane molecules

Table 2. Oxidation of styrene over catalysts OMCA-x and Co/OMA-10 prepared with different methods.

Catalyst	Solvent	Conversion (%)	Selectivity (%)		
			Styrene oxide	Benzaldehyde	TOF (h^{-1})
OMA	1,4-dioxane	25.8	18.4	51.9	--
Co/OMA-10	1,4-dioxane	36.8	17.8	68.9	21.0
OMCA-30	1,4-dioxane	64.6	49.1	44.2	110.7
OMCA-20	1,4-dioxane	72.2	52.4	39.0	82.4
OMCA-10	1,4-dioxane	75.8	56.6	34.7	43.3
2rd Recycle	1,4-dioxane	70.6	55.6	31.5	40.3
3rd Recycle	1,4-dioxane	68.9	55.8	34.3	39.4
OMCA-5	1,4-dioxane	78.8	50.4	35.4	22.5
OMCA-10	methylbenzene	33.9	23.9	76.1	19.4

coordinated to the cobalt cations through oxygen atoms, and further be transferred to active sites Ia type Al-OH species to create the superficial hydroperoxides (Al-OOH), at which the styrene molecules are selectively oxidized to styrene oxide. While, the reactant styrene molecules reacted directly with Co(III)-$OO^{\cdot}$ superoxo type complex rather than superficial Al-OOH are mainly oxidized into benzaldehyde with a small quantity of styrene oxide. Furthermore, Co_3O_4 nanoparticles themselves also may catalyze the formation of an acylperoxy radical from benzaldehyde by O_2, which can oxidize styrene to give styrene oxide and benzoic acid.[55, 67, 68] Consequently, the special catalyst OMCA-5 containing highly homogeneously dispersed Co_3O_4 nanoparticles within mesoporous walls or channels (Fig. 3c and Fig. 8) still exhibited a higher epoxidation productivity than that of catalyst Co/OMA-10, while, the productivity of benzoic acid as the main by-product over catalyst OMCA-5 was higher than those of other catalysts OMCA-x. In order to confirm this assumption, we have carried out the oxidation of styrene with the use of OMCA-10 and methylbenzene as catalyst and solvent, respectively. Due to the incapability to transfer the radical-type active oxygens from solvent methylbenzene, the conversion of styrene was only 33.9% under the same reaction conditions with the selectivities for styrene oxide and benzaldhyde being 23.9% and 76.1%, respectively. Clearly, during the whole epoxidation reaction of styrene over cobalt-alumina catalysts, the amount of Ia type Al-OH species plays pivotal role in improving the selectivity to styrene oxide, and solvent 1,4-dioxane molecules are the key factor responsible for the transmission of free-radical-type active oxygens from oxygen activated by four-coordinated Co^{2+} cations to labile Ia type Al-OH active sites, at which the ligand exchange of -OH by -OOH is kinetically very fast.[13]

The Knözinger and Ratnasamy model proposes that the (111), (110), and (100) faces of alumina are covered by hydroxyl with five configurations (types Ia, Ib, IIa, IIb, and III).[69] By correlating the total density of each hydroxyl type with the equivalent number of AlO_x sites in the bulk alumina, the terminal-hydroxyl is mainly the Ia type Al-OH bonded with four-coordinated Al(III) ions.[13] Via the evaporation-induced triconstituent cooperative co-assembly method proposed by us, the homogeneous incorporation of tetrahedrally coordinated cobalt(II) and the formation Co-O-Al bond can effectively increase the content of tetra-coordinated framework aluminum (Fig. 9), and inevitably facilitate the formation of the Ia type Al-OH sites, leading to a higher selectivity to styrene oxide over OMCA-x than those of OMA and Co/OMA-10 (Table 2). Noteworthily, with increasing the loading of Co, the increased four-coordinated Co^{2+} cations locating at surface or near-surface of mesoporous pores can remarkably enhance the ability to activate oxygen in catalysts OMCA-x, which is responsible for the increased conversion of styrene from 64.6% to 78.8%, for OMCA-30 and OMCA-5, respectively (Table 2). However, the elimination of excess cobalt species from the mesoporous framework of alumina would necessarily result in the part collapse of ordered mesostructure of OMCA-5 (Fig. 2a and Fig. 3c), and

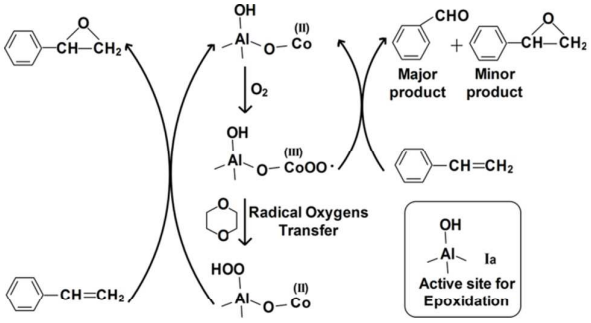

Fig. 10 Proposed tentative reaction mechanism for the epoxidation of styrene over catalysts OMCA-x.

consequentially decrease the content of tetra-coordinated framework aluminum (Fig. 9), which could be explained to the distinct reduction in the selectivity to styrene oxide.

Repeated runs of the recovered OMCA-10 for the epoxidation of styrene have been carried out to explain its superior reusability. From Table 2, it can be seen that over the recycled catalyst OMCA-10, neither styrene conversion nor epoxide selectivity changed significantly in the repeated runs. Even after the third run, the conversion of styrene over catalyst OMCA-10 was still 68.9 % with the selectivity for styrene oxide of 55.8%. When the atomic absorption spectroscopy was carried out to determine the retained content of cobalt species in the reused catalyst OMCA-10 after the third cycle, the cobalt content was high as 6.20 wt % with only a 1.59 % decrease compared with the as-prepared OMCA-10. In addition, the hot filtration test was also carried out to further test the leaching amount of Co from the solid catalyst OMCA-10 during the reaction. After the reaction, the solid catalyst was filtered out under hot conditions. Then, the filtrate was treated with aqua regia several times and the mixture was evaporated to remove the organic part. After preparing the aqueous solution of the filtrate, it was subjected to atomic absorption spectroscopic analysis. The result showed that compared with the as-prepared OMCA-10, only 1.31% of

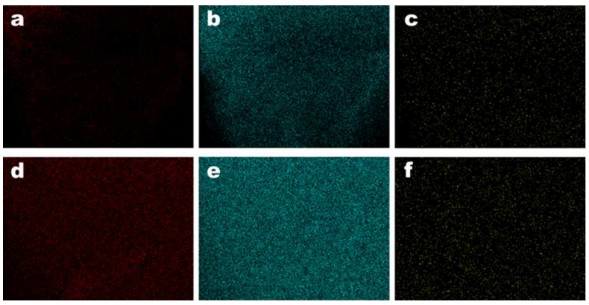

Fig. 11 Elemental analysis mapping for two different regions of recycled catalyst OMCA-10 after the third run showing the distributions of O (a, d), Al (b, e), and Co (c, f). Maps in each row are for the same region.

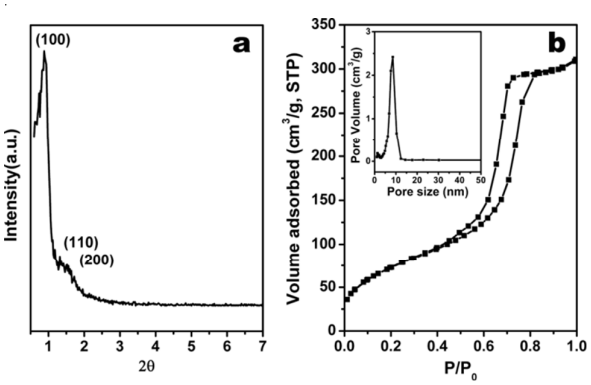

Fig. 12 XRD pattern (a) and the N_2 isotherm (b) of recycled catalyst OMCA-10 after the third cycle (the inset in b is the corresponding pore size distribution curve).

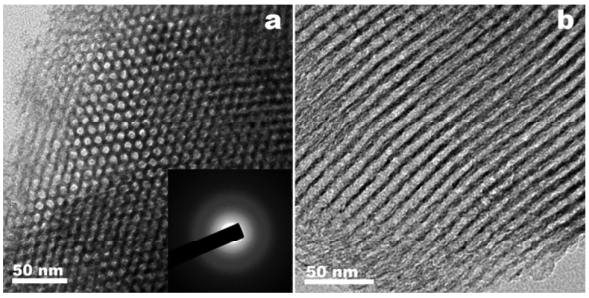

Fig. 13 TEM images (a) and (b) of recycled catalyst OMCA-10 after the third cycle viewed along [110] and [100] directions, respectively (the inset in a is the corresponding SAED pattern).

Co was leached out to the solution phase during the reaction at 90 ^{o}C. These results indicated that the strong interaction between aluminium and cobalt species within mesoporous framework (Fig. 8) can effectively inhibit the leaching of active cobalt species. In addition, the homogeneous distribution of the elements within the framework of reused catalyst OMCA-10 was further confirmed by the density of the O, Al, and Co spots in the elemental mapping (Fig. 11). Semiquantitative composition analysis indicate that the atomic ratio of aluminium to cobalt were 13.6 and 12.9, respectively, when two different regions were selected, which are close to the initial value in catalyst OMCA-10.

The superior reusability of catalyst OMCA-10 could also be attributed to its excellent mesostructural stability, which can be characterized by using XRD, TEM, and N_2 physisorption. Fig. 12 showed the XRD pattern and N_2 adsorption-desorption isotherm of recycled catalyst OMCA-10 after the third cycle. From the small-angle XRD pattern of reused catalyst OMCA-10, it can be seen that similar to as-prepared catalyst OMCA-10 (Fig. 2a), the recycled catalyst OMCA-10 still displayed two well-resolved Bragg diffraction peaks (Fig. 12a), indicating that the highly ordered mesostructure was well maintained. Moreover, little change can be observed in the N_2 adsorption-desorption isotherms for catalyst OMCA-10 before (Fig. 5a) and after the third reaction (Fig. 12b). Compared to the as-prepared OMCA-10 (Table 1), the decreases in BET surface area and total pore volume only were 5.8% and 14.7%, respectively. Furthermore, for the recycled catalyst OMCA-10, the hexagonal honeycomb-like mesopores along [100] direction and uniform cylindrical mesopores along [110] direction can also be seen from TEM images displayed in Fig. 13a and 13b, respectively, showing a highly ordered 2D hexagonal mesoporous ordering, which is in good agreement with its type IV isotherm with H1-tpye hysteresis loop and

Table 3. Comparison of OMCA-10 with the earlier reported cobalt-containing heterogeneous catalysts for the styrene epoxidation reaction using O_2 as oxidant without adding any initiator.

Entry	Catalyst	Temperature (^{o}C)	Conversion (%)	Selectivity (%)	TOF (h^{-1})	Ref.
1	Co-ZSM-5(L_2)	90	27.2	45.6	10.2	[70]
2	Co/γ-Al_2O_3	100	33.1	44.7	3.5	[71]
3	Mg/Co/Al-2	95	38.1	36.0	24.5	[66]
4	Co/TS-1	100	38.5	49.2	15.3	[71]
5	Co/SBA-15	100	43.5	55.6	5.2	[29]
6	Co^{2+}-NaX	100	44.0	60.0	4.7	[55]
7	Co^{2+}-MCM-41	100	45.0	62.0	54.1	[55]
8	ZC-700	90	41.9	75.4	14.0	[72]
9	Co-MCM-41	80	50.0	90.0	29.5	[73]
10	Co/HMS	100	63.0	51.0	39.6	[74]
11	Co-HMS-X	120	90.0	59.8	30.3	[75]
12	γ-Fe_2O_3@SiO_2-NH_2-Co(acac)$_2$	110	82.0	98.0	5.4	[76]
13	Co-SBA-15	100	94.1	65.5	11.2	[29]
14	Co/CNTs(in)	100	99.1	92.8	79.6	[77]
15	OMCA-10	90	75.8	56.6	43.3	This work

narrow pore size distribution (Fig. 12b). It is worth noting that there was no obvious large and aggregated cobalt oxides observed, which further confirmed that the confinement effect of the mesoporous framework of alumina played an important role in stabilizing the Co active species against aggregation and crystallization during catalytic reaction. All of these results indicate that OMCA-10 prepared by our method exhibits high stability and highly ordered mesostructure even after being used for three cycles of styrene epoxidation reaction.

The catalytic performance of OMCA-10 catalyst was compared with the earlier reported containing-cobalt heterogeneous catalysts[29, 55, 66, 70-77] for epoxidation of styrene using O_2 as oxidant without adding any initiator (Table 3). Obviously, catalyst OMCA-10 shows the relatively higher TOF value for catalytic epoxide production or comparable to the earlier reports (except for Co/CNTs(in)), and the styrene conversion and yield of styrene oxide over OMCA-10 are better than those of catalysts listed in entry 1-10 of Table 3. Although 90.0% of styrene conversion was obtained over Co-HMS-X (Table 3, entry 11), the higher reaction temperature (120 ^{o}C) was needed. Even so, the selectivity to styrene oxide was only 59.8%, which is slightly higher than that of catalyst OMCA-10. Furthermore, from entry 12-14, catalysts γ-Fe_2O_3@SiO_2-NH_2-Co(acac)$_2$, Co-SBA-15 and CoCNTs(in) can achieve satisfactory styrene conversion and epoxide selectivity, however, synthetic processes of these catalysts are very complicated. For example, the synthesis of Co-SBA-15 involves twice crystallizing at 100^{o}C for 2 days. Moreover, during the whole synthetic period, it is indispensable to adjust pH of synthesis system being 7.5. The comparison results corroborate that catalyst OMCA-10 prepared with our method acts as an efficient catalyst for epoxidation of styrene using O_2 as oxidant.

4. Conclusions

The highly ordered mesoporous cobalt-alumina catalysts (OMCA-x) with high surface area and uniformly distributed mesopores have been successfully synthesized via a low temperature EISA pathway associated with thermal treatment to promote the cooperative co-assembly between F127 and aluminum/cobalt species. Using such method, almost all cobalt species could be highly homogeneously incorporated into alumina mesoporous framework in the form of tetrahedrally coordinated divalent Co-oxide moieties. The homogeneous incorporation of Co and the formation of Co-O-Al bond could be responsible for the increased mesostructural ordering of OMCA-x and a remarkable increase in the content of tetra-coordinated framework aluminum. For the epoxidation of styrene, a synergetic effect of highly homogeneously dispersed Co^{2+} in tetrahedral position and Ia type Al-OH sites bonded to four-coordinated Al(III) ions is proposed to explain the much higher conversion of styrene and epoxide productivity over catalysts OMCA-x than those of support OMA and Co/OMA-10 prepared by the traditional IWI method. Especially, catalyst OMCA-10 exhibits the excellent catalytic properties for the epoxidation reaction, i.e., a conversion of 75.8% with the highest selectivity to styrene oxide (56.6%). Most strikingly, the highly ordered mesostructure of catalyst OMCA-10 can be well maintained even after the third epoxidation of styrene with only a 5.8% decrease in its BET surface area. In addition, the strong interaction between cobalt and aluminium species in mesoporous framework can effectively inhibit the leaching of active cobalt species. As a result, catalyst OMCA-10 exhibits an excellent recyclable stability without significant loss of activity and selectivity within three successive runs. Our achievements provide new contributions to synthesize active transition-metal-doped OMA, taking advantage of both the properties of OMA and the enhanced catalytic activity of transition metal, which may further extend the catalytic application for various reactions in petroleum and petrochemical industry.

Acknowledgements

This work was financially supported by the National Natural Science Foundation of China (51172154, 51451002, and 21406153), the Shanxi Province Science Foundation for Youths (2012021006-2, 2013021008-3, and 2014021014-2), and the Science and Technology Project of Shanxi Province (20130313001-3).

References

1. Y. Yang, H. Ding, S. J. Hao, Y. Zhang and Q. B. Kan, *Appl. Organomet. Chem.*, 2011, **25**, 262-269.
2. J. Sebastian, K. M. Jinka and R. V. Jasra, *J. Catal.*, 2006, **244**, 208-218.
3. P. Pal, S. K. Pahari, A. Sinhamahapatra, M. Jayachandran, G. V. M. Kiruthika, H. C. Bajaj and A. B. Panda, *RSC Adv.*, 2013, **3**, 10837-10847.
4. A. Patel and S. Pathan, *Ind. Eng. Chem. Res.*, 2012, **51**, 732-740.
5. Y. M. Liu, H. Tsunoyama, T. Akita and T. Tsukuda, *Chem. Commun.*, 2010, **46**, 550-552.
6. W. C. Zhan, Y. L. Guo, Y. Q. Wang, Y. Guo, X. H. Liu, Y. S. Wang, Z. G. Zhang and G. Z. Lu, *J. Phys. Chem. C*, 2009, **113**, 7181-7185.
7. L. Espinal, S. L. Suib and J. F. Rusling, *J. Am. Chem. Soc.*, 2004, **126**, 7676-7682.
8. S. B. Kumar, S. P. Mirajkar, G. C. G. Pais, P. Kumar and R. Kumar, *J. Catal.*, 1995, **156**, 163-166.
9. S. C. Laha and R. Kumar, *J. Catal.*, 2001, **204**, 64-70.
10. B. T. Li, X. J. Jin, Y. R. Zhu, L. Chen, Z. J. Zhang and X. J. Wang, *Inorg. Chim. Acta*, 2014, **419**, 66-72.
11. R. Van Grieken, J. L. Sotelo, C. Martos, J. L. G. Fierro, M. López-Granados and R. Mariscal, *Catal. Today*, 2000, **61**, 49-54.
12. Y. Zhu, R. C. Jin and Y. H. Sun, *Int. J. Hydrog. Energy*, 2013, **38**, 16716-16721.
13. R. Rinaldi, F. Y. Fujiwara, W. Holderich and U. Schuchardt, *J. Catal.*, 2006, **244**, 92-101.

14. W. Lueangchaichaweng, L. Li, Q. Y. Wang, B. L. Su, C. Aprile and P. P. Pescarmona, *Catal. Today*, 2013, **203**, 66-75.
15. M. R. Maurya, A. K. Chandrakar and S. Chand, *J. Mol. Catal. A-Chem.*, 2007, **274**, 192-201.
16. M. R. Maurya, A. K. Chandrakar and S. Chand, *J. Mol. Catal. A-Chem.*, 2007, **270**, 225-235.
17. J. Chakraborty, M. Nandi, H. Mayer-Figge, W. S. Sheldrick, L. Sorace, A. Bhaumik and P. Banerjee, *Eur. J. Inorg. Chem.*, 2007, **32**, 5033-5044.
18. W. C. Zhan, Y. L. Guo, Y. Q. Wang, X. H. Liu, Y. Guo, Y. S. Wang, Z. G. Zhang and G. Z. Lu, *J. Phys. Chem. B*, 2007, **111**, 12103-12110.
19. S. Gómez, L. J. Garces, J. Villegas, R. Ghosh, O. Giraldo and S. L. Suib, *J. Catal.*, 2005, **233**, 60-67.
20. M. Nandi, P. Roy, H. Uyama and A. Bhaumik, *Dalton Trans.*, 2011, **40**, 12510-12518.
21. M. J. Rak, M. Lerro and A. Moores, *Chem. Commun.*, 2014, **50**, 12482-12485.
22. L. X. Zhang, Z. L. Hua, X. P. Dong, L. Li, H. R. Chen and J. L. Shi, *J. Mol. Catal. A-Chem.*, 2007, **268**, 155-162.
23. T. Ohno, Y. Masaki, S. Hirayama and M. Matsumura, *J. Catal.*, 2001, **204**, 163-168.
24. T. Nguyen Tien and T. Ho Huu, *Catal. Commun.*, 2014, **45**, 153-157.
25. V. Parvulescu and B. L. Su, *Catal. Today*, 2001, **69**, 315-322.
26. M. Popova, Á. Szegedi, K. Lázár and Z. Károly, *Micropor. Mesopor. Mat.*, 2012, **151**, 180-187.
27. B. Tang, X. H. Lu, D. Zhou, J. Lei, Z. H. Niu, J. Fan and Q. H. Xia, *Catal. Commun.*, 2012, **21**, 68-71.
28. B. T. Li, Y. R. Zhu and X. J. Jin, *J. Solid State Chem.*, 2015, **221**, 230-239.
29. H. T. Cui, Y. Zhang, Z. G. Qiu, L. F. Zhao and Y. L. Zhu, *Appl. Catal. B-Environ.*, 2010, **101**, 45-53.
30. H. J. Zhan, Q. H. Xia, X. H. Lu, Q. Zhang, H. X. Yuan, K. X. Su and X. T. Ma, *Catal. Commun.*, 2007, **8**, 1472-1478.
31. J. M. Zhang, A. V. Biradar, S. Pramanik, T. J. Emge, T. Asefa and J. Li, *Chem. Commun.*, 2012, **48**, 6541-6543.
32. X. X. Gao, C. J. Huang, N. W. Zhang, J. H. Li, W. Z. Weng and H. L. Wan, *Catal. Today*, 2008, **131**, 211-218.
33. S. Suvanto, J. Hukkamäki, T. T. Pakkanen and T. A. Pakkanen, *Langmuir*, 2000, **16**, 4109-4115.
34. B. Y. Jibril and S. Ahmed, *Catal. Commun.*, 2006, **7**, 990-996.
35. S. Todorova, V. Parvulescu, G. Kadinov, K. Tenchev, S. Somacescu and B. L. Su, *Micropor. Mesopor. Mat.*, 2008, **113**, 22-30.
36. Y. Kim, C. Kim, I. Choi, S. Rengaraj and J. Yi, *J. Environ. Sci. Technol.*, 2004, **38**, 924-931.
37. D. Gu and F. Schuth, *Chem. Soc. Rev.*, 2014, **43**, 313-344.
38. X. Y. Wang, D. H. Pan, M. Guo, M. He, P. Y. Niu and R. F. Li, *Mater. Lett.*, 2013, **97**, 27-30.
39. B. Y. Huang, C. H. Bartholomew, S. J. Smith and B. F. Woodfield, *Micropor. Mesopor. Mat.*, 2013, **165**, 70-78.
40. B. Y. Huang, C. H. Bartholomew and B. F. Woodfield, *Micropor. Mesopor. Mat.*, 2013, **177**, 37-46.
41. Z. X. Wu, Q. A. Li, D. Peng, P. A. Webley and D. Y. Zhao, *J. Am. Chem. Soc.*, 2010, **132**, 12042-12050.
42. Q. Liu, A. Q. Wang, X. D. Wang and T. Zhang, *Chem. Mater.*, 2006, **18**, 5153-5155.
43. H. F. Yang and D. Y. Zhao, *J. Mater. Chem.*, 2005, **15**, 1217-1231.
44. Q. Yuan, A. X. Yin, C. Luo, L. D. Sun, Y. W. Zhang, W. T. Duan, H. C. Liu and C. H. Yan, *J. Am. Chem. Soc.*, 2008, **130**, 3465-3472.
45. S. Ghosh and M. K. Naskar, *J. Am. Ceram. Soc.*, 2014, **97**, 100-106.
46. C. Marquez-Alvarez, N. Zilkova, J. Perez-Pariente and J. Cejka, *Catal. Rev.-Sci. Eng.*, 2008, **50**, 222-286.
47. K. Niesz, P. D. Yang and G. A. Somorjai, *Chem. Commun.*, 2005, 1986-1987.
48. W. Q. Cai, J. G. Yu, C. Anand, A. Vinu and M. Jaroniec, *Chem. Mater.*, 2011, **23**, 1147-1157.
49. Z. X. Li, F. B. Shi, L. L. Li, T. Zhang and C. H. Yan, *Phys. Chem. Chem. Phys.*, 2011, **13**, 2488-2491.
50. Q. Yuan, H. H. Duan, L. L. Li, Z. X. Li, W. T. Duan, L. S. Zhang, W. G. Song and C. H. Yan, *Adv. Mater.*, 2010, **22**, 1475-1478.
51. Y. Bang, S. J. Han, J. G. Seo, M. H. Youn, J. H. Song and I. K. Song, *Int. J. Hydrog. Energy*, 2012, **37**, 17967-17977.
52. D. H. Pan, M. Guo, M. He, S. W. Chen, X. Wang, F. Yu and R. F. Li, *J. Mater. Res.*, 2014, **29**, 811-819.
53. F. Rashidi, A. N. Kharat, A. M. Rashidi, E. Lima, V. Lara and J. S. Valente, *Eur. J. Inorg. Chem.*, 2010, 1544-1551.
54. Y. H. Zhang, F. Gao, H. Q. Wan, C. Wu, Y. Kong, X. C. Wu, B. Zhao, L. Dong and Y. Chen, *Micropor. Mesopor. Mat.*, 2008, **113**, 393-401.
55. Q. H. Tang, Q. H. Zhang, H. L. Wu and Y. Wang, *J. Catal.*, 2005, **230**, 384-397.
56. L. F. Liotta, G. Pantaleo, A. Macaluso, G. Di Carlo and G. Deganello, *Appl. Catal. A-Gen.*, 2003, **245**, 167-177.
57. H. F. Xiong, Y. H. Zhang, K. Liew and J. L. Li, *J. Mol. Catal. A-Chem.*, 2005, **231**, 145-151.
58. P. Arnoldy and J. A. Moulijn, *J. Catal.*, 1985, **93**, 38-54.
59. J. S. Beck, J. C. Vartuli, W. J. Roth, M. E. Leonowicz, C. T. Kresge, K. D. Schmitt, C. T. W. Chu, D. H. Olson and E. W. Sheppard, *J. Am. Chem. Soc.*, 1992, **114**, 10834-10843.
60. A. Firouzi, D. Kumar, L. M. Bull, T. Besier, P. Sieger, Q. Huo, S. A. Walker, J. A. Zasadzinski, C. Glinka, J. Nicol and a. et, *Science*, 1995, **267**, 1138-1143.
61. F. Dumeignil, M. Rigole, M. Guelton and J. Grimblot, *Chem. Mater.*, 2005, **17**, 2361-2368.
62. T. P. Xiu, J. C. Wang and Q. Liu, *Micropor. Mesopor. Mat.*, 2011, **143**, 362-367.
63. P. J. Chupas and C. P. Grey, *J. Catal.*, 2004, **224**, 69-79.
64. B. Corzilius, V. K. Michaelis, S. A. Penzel, E. Ravera, A. A. Smith, C. Luchinat and R. G. Griffin, *J. Am. Chem. Soc.*, 2014, **136**, 11716-11727.
65. H. Knözinger and P. Ratnasamy, *Rev.-Sci. Eng.*, 1978, **17**, 31-70.
66. N. T. Thao and H. H. Trung, *Catal. Commun.*, 2014, **45**, 153-157.
67. R. Raja, G. Sankar and J. Meurig Thomas, *Chem. Commun.*, 1999, 829-830.
68. Z. F. Li, S. J. Wu, Y. Y. Ma, H. Liu, J. Hu, L. L. Liu, Q. S. Huo, J. Q. Guan and Q. B. Kan, *Transit. Met. Chem.*, 2013, **38**, 243-251.

69. Y. Amenomiya, Y. Morikawa and G. Pleizier, *J. Catal.*, 1977, **46**, 431-433.
70. G. Xu, Q. H. Xia, X. H. Lu, Q. Zhang and H. J. Zhan, *J. Mol. Catal. A-Chem.*, 2007, **266**, 180-187.
71. J. Jiang, R. Li, H. L. Wang, Y. F. Zheng, H. N. Chen and J. T. Ma, *Catal. Lett.*, 2008, **120**, 221-228.
72. G. L. Yu, J. Sun, F. Muhammad, P. Y. Wang and G. S. Zhu, *RSC Adv.*, 2014, **4**, 38804-38811.
73. S. Bhunia, S. Jana, D. Saha, B. Dutta and S. Koner, *Catal. Sci. Technol.*, 2014, **4**, 1820-1828.
74. Z. Q. Shi, L. X. Jiao, J. Sun, Z. B. Chen, Y. Z. Chen, X. H. Zhu, J. H. Zhou, X. C. Zhou, X. Z. Li and R. Li, *RSC Adv.*, 2014, **4**, 47-53.
75. S. Rahman, C. Santra, R. Kumar, J. Bahadur, A. Sultana, R. Schweins, D. Sen, S. Maity, S. Mazumdar and B. Chowdhury, *Appl. Catal. A-Gen*, 2014, **482**, 61-68.
76. X. Z. Li, Y. Y. Fang, X. C. Zhou, J. T. Ma and R. Li, *Mater. Chem. Phys.*, 2015, **156**, 9-15.
77. Z.-Q. Shi, Z.-P. Dong, J. Sun, F.-W. Zhang, H.-L. Yang, J.-H. Zhou, X.-H. Zhu and R. Li, *Chem. Eng. J*, 2014, **237**, 81-87.

Facile synthesis of highly ordered mesoporous cobalt-alumina catalysts and their application in liquid phase selective oxidation of styrene

Dahai Pan,* Qian Xu, Zhaoyang Dong, Shuwei Chen, Feng Yu, Xiaoliang Yan, Binbin Fan and Ruifeng Li *

The Research Center of Chemical Technology & Catalysis for Energy, College of Chemistry and Chemical Engineering, Taiyuan University of Technology, Taiyuan 030024, P. R. China.

A schematic procedure to illustrate the preparation of highly ordered mesoporous cobalt-alumina catalysts with highly homogeneously dispersed Co(II) species via the evaporation-induced triconstituent cooperative co-assembly method.

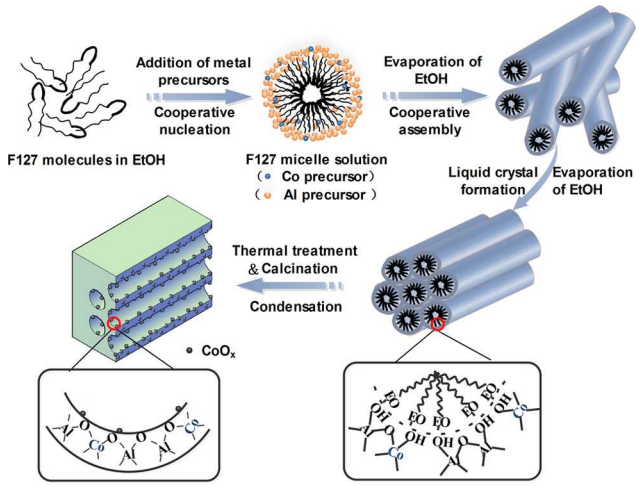

* Corresponding authors. Fax: +86-351-6010121, e-mail: pandahai@foxmail.com (D. H. Pan); rfli@tyut.edu.cn (R. F. Li).